DOI: 10.3901/CJME.2015.0206.054, available online at www.springerlink.com; www.cjmenet.com; www.cjme.com.cn

Numerical Modeling of a Spar Platform Tethered by a Mooring Cable

ZHU Xiangqian and YOO Wan-Suk*

Computer Aided Engineering Laboratory, School of Mechanical Engineering, Pusan National University, Busan 609735, Korea

Received September 18, 2014; revised January 26, 2015; accepted February 6, 2015

Abstract: Virtual simulation is an economical and efficient method in mechanical system design. Numerical modeling of a spar platform, tethered by a mooring cable with a spherical joint is developed for the dynamic simulation of the floating structure in ocean. The geometry modeling of the spar is created using finite element methods. The submerged part of the spar bears the buoyancy, hydrodynamic drag force, and effect of the added mass and Froude-Krylov force. Strip theory is used to sum up the forces acting on the elements. The geometry modeling of the cable is established based on the lumped-mass-and-spring modeling through which the cable is divided into 10 elements. A new element-fixed local frame is used, which is created by the element orientation vector and relative velocity of the fluid, to express the loads acting on the cable. The bottom of the cable is fixed on the seabed by spring forces, while the top of the cable is connected to the bottom of the spar platform by a modified spherical joint. This system suffers the propagating wave and current in the *X*-direction and the linear wave theory is applied for setting of the propagating wave. Based on the numerical modeling, the displacement-load relationships are analyzed, and the simulation results of the numerical modeling are compared with those by the commercial simulation code, ProteusDS. The comparison indicates that the numerical modeling of the spar platform tethered by a mooring cable is well developed, which provides an instruction for the optimization of a floating structure tethered by a mooring cable system.

Keywords: numerical modeling, dynamic simulation, spar platform, mooring cable, spherical joint

1 Introduction

The exploitation and utilization of marine resources and the development of the marine industry have always been international concerned[1–2]. These processes are closely connected with the development of computer technology. Virtual simulations based on the mathematical modeling and computer technology are becoming more and more popular in the fields of mechanical and marine engineering[3–5] in recent decades. A tethered buoy system is widely used for meteorology monitoring and navigation systems in the marine engineering domain. It is a typical multibody system, and the dynamic behavior of spar platform with catenary mooring system was analyzed by AGARWAL and JAIN[6]. A theoretical analysis on the unstable oscillation of moored buoy was reported by IDRIS, et al[7]. With the development of computer-aided engineering, more extensive numerical modeling has been established and analyzed. Theoretical and experimental analyses of a tethered spherical buoy were reported by RADHAKRISHNAN, et al[8] , and spar platforms have been widely used for oil and gas production facilities[9–10]. Moreover, a spar platform tethered by a cable system was studied for designing floating offshore wind turbines by ZHU and JONKMAN, et al[11–12] in recent years. Generally, this system can be simply divided into three parts: the spar platform, mooring cable, and constraints. Cable modeling was also proposed, in which a new reference frame was created for each cable element by ZHU, et al[13–14]. This new reference frame was established based on the element orientation vector and relative velocity of the fluid. The formulations of both the rotational transformation matrix and external forces are effectively expressed with the application of the new reference frame. To complete the system of a three-dimensional spar platform tethered by a mooring cable, the spar modeling and constraint modeling are put forward in this paper. The spar platform is assembled using 20 cylinder elements placed head-to-tail in the vertical direction. It is assumed that the relative velocity and acceleration do not change within one element, and the external loads are acting on the central points of the elements. The loads are composed of the buoyancy, hydrodynamic drag forces, effect of the added mass, and the Froude-Krylov force. The buoyancy is carried out by integrating the submerged volume. The rest external forces are determined by summing up the loads acting on each

* Corresponding author. E-mail: wsyoo@pusan.ac.kr

Supported by Human Resources Development Program of Korea Institute of Energy Technology Evaluation and Planning(KETEP), Ministry of Trade, Industry and Energy of Korea(Grant No. 20134030200290)

element with respect to the local frame of the spar. The relative moment forces are added during the summation. The bottom of the cable is connected to the seabed by spring forces with respect to the *X*-, *Y*-, and *Z*-directions. These spring forces are linear functions of the relative positions and velocities between the bottom node of the cable and anchor point on the seabed. A three-by-three coefficient-matrix is applied to determine the spring forces. The top of the cable is connected to the bottom of the spar platform by a spherical joint which is modified to be appropriate for the connection between a mass point and a three-dimensional body. The linear wave theory is applied to express the *X*-directional wave[15]. The current is set as a constant speed of fluid in the *X*-direction. Finally, the displacement-load relationship is analyzed and the simulation results for this numerical modeling are verified by comparing them with those from the commercial simulation code ProteusDS, which is widely used for simulating the floating platform and cable systems[16–17]. This numerical modeling of the spar platform tethered by a mooring cable is well developed which is illustrated by the simulation results.

2 Modeling

The origin of the global reference frame lies at the still water level. The *X*-axis points to the east, while the *Z*-axis points vertically upward. Thus, the *Y*-axis points to the north according to the right hand rule, as shown by Fig. 1. This system is developed based on the numerical modeling, which includes the spar modeling, cable modeling, and constraint modeling. These are described separately in the following sections, and the modeling of the cable and wave can be found in detail in Refs. [13–15, 18–22].

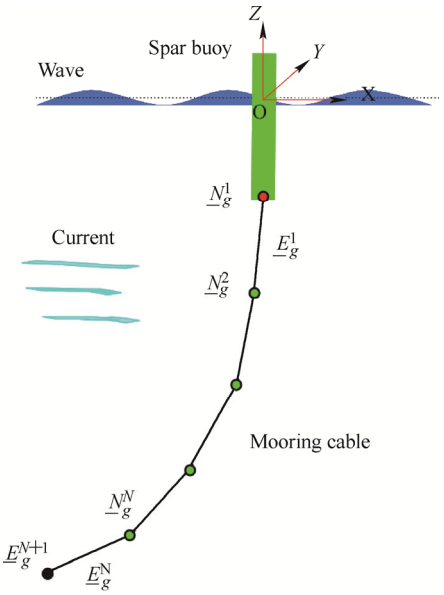

Fig. 1.　Floating spar platform fastened by a cable

2.1 Spar modeling

The origin of the local frame of the spar is located at the geometric center of the spar platform, and the directions of the axes coincide with those of the global reference frame system at the initial condition. The initial position of the spar is chosen as its undisplaced position in the wave. The spar modeling is axially-, radially- and angularly-divided in ProteusDS, as shown in Fig. 2. While, it is evenly divided into 20 elements axially in the numerical modeling, as shown in Fig. 3. The geometry data of the spar modeling is listed in Table 1.

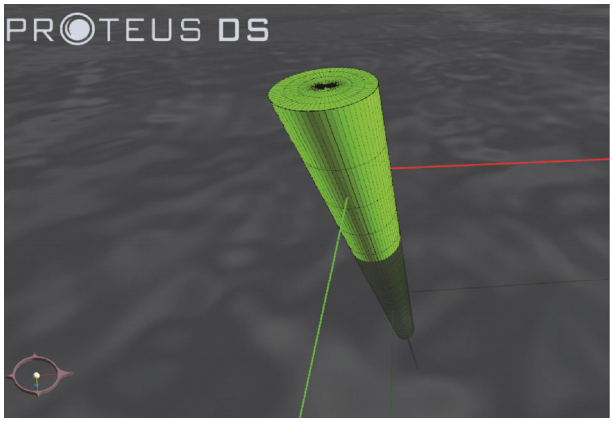

Fig. 2.　Spar modeling in ProteusDS

Table 1.　Properties of spar

Parameter	Value
Diameter D^{b}/m	0.4
Mass M^{b}/kg	500
Length L^{b}/m	5
Center of mass CM/m	–2
Drag coefficient C_D^{b}	1
Added-mass coefficient C_A^{b}	0.5
Cross-area A^{b}/m^2	0.126

The external forces acting on the spar platform are denoted by $\underline{F}^{\mathrm{b}}$, as shown in Eq. (1). They are composed of three parts: the buoyancy and gravity force $\underline{F}_B^{\mathrm{b}}$, the effect of the added-mass and Froude-Krylov force $\underline{F}_A^{\mathrm{b}}$, and the hydrodynamic drag forces $\underline{F}_D^{\mathrm{b}}$:

$$\underline{F}^{\mathrm{b}} = \underline{F}_B^{\mathrm{b}} + \underline{F}_A^{\mathrm{b}} + \underline{F}_D^{\mathrm{b}}. \tag{1}$$

2.1.1 *Buoyancy*

The buoyancy comes from the pressure acting on the surface components contacting with the fluid. The magnitude is equal to the weight of the displaced fluid, and the center of the gravity is collinear with the center of the buoyancy in the vertical direction. Therefore, the gravity of the spar is expressed together with the buoyancy in this paper. In view of the continually changing of the center of the buoyancy and the column shape of the platform, the buoyancy and gravity of the spar are expressed as Eq. (2):

$$\underline{F}_B^{\mathrm{b}} = \rho_{\mathrm{f}} g V_0 \underline{\delta}_{i3} - M^{\mathrm{b}} \underline{g} + \underline{\underline{C}}^{\mathrm{b}} \underline{q}^{\mathrm{b}}. \tag{2}$$

The first term on the right-hand side represents the buoyancy at the initial position, which is equal to the weight of the displaced fluid. The vector $\underline{\delta}_{i3}$ indicates the X- and Y-components of the vector $\rho g V_0 \underline{\delta}_{i3}$ being zero. The second term is the weight of the spar platform. Finally, the last term represents the change of the buoyancy and restoring moments as the spar is displaced. Matrix $\underline{\underline{C}}^{\mathrm{b}}$ depends on the geometry of the spar and is shown by

$$\underline{\underline{C}}^{\mathrm{b}} = \begin{pmatrix} 0 & 0 & 0 & 0 & 0 & 0 \\ 0 & 0 & 0 & 0 & 0 & 0 \\ 0 & 0 & 1.26\times10^{3} & 0 & 0 & 0 \\ 0 & 0 & 0 & -9.52\times10^{3} & 0 & 0 \\ 0 & 0 & 0 & 0 & -9.52\times10^{3} & 0 \\ 0 & 0 & 0 & 0 & 0 & 0 \end{pmatrix}. \tag{3}$$

2.1.2 Added-mass and Froude-Krylov effect

The added mass represents the effects coming from the relative acceleration between the wave particles and spar, and the Froude-Krylov force represent the pressure effects of the undisturbed incident waves as shown in

$$\underline{F}_A^{\mathrm{b}} = \left(1 + C_A^{\mathrm{b}}\right) V_{\mathrm{s}} \rho_{\mathrm{f}} \bullet \underline{\dot{V}}_g^{f} - C_A^{\mathrm{b}} V_{\mathrm{s}} \rho_{\mathrm{f}} \underline{\ddot{q}}_g^{\mathrm{b}}. \tag{4}$$

where C_A^{b} is the coefficient of the added-mass normal to the geometry of the cable, V_s denotes the submerged volume of the spar platform and is carried out by summing the submerged spar elements, $\underline{\dot{V}}_g^{\mathrm{f}}$ is the acceleration of the surrounding fluid particles, and $\underline{\ddot{q}}_g^{\mathrm{b}}$ represents the acceleration of the spar elements.

2.1.3 Hydrodynamic drag force

According to the definition, the drag forces are a quadratic function of the relative velocity of the fluid. The hydrodynamic drag forces are expressed by

$$\underline{F}_D^{\mathrm{b}} = -\frac{1}{2} C_D^{\mathrm{b}} \rho_f A^{\mathrm{b}} \left\| \underline{V}_g^R \right\| \underline{V}_g^R. \tag{5}$$

Strip theory is used to sum up the hydrodynamic pressure, effect of the added mass and Froude-Krylov force acting on the total surface of the spar elements. These forces are expressed with respect to the local frame of the spar and concentrated at the center of each element. The moment forces, as shown by Eq. (6), are added to translate the forces acting on the elements to the origin of the spar frame:

$$M_A^{\mathrm{b}} = \sum_{j=1}^{M} \left({}^{j,1}F_A^{\mathrm{b}} \bullet {}^{j,3}q^{\mathrm{b}} + {}^{j,1}F_D^{\mathrm{b}} \bullet {}^{j,3}q^{\mathrm{b}} \right). \tag{6}$$

where ${}^{j,1}F_A^{\mathrm{b}}$ is the *1*st value of the *j*th vector $\underline{F}_A^{\mathrm{b}}$, and ${}^{j,3}q^{\mathrm{b}}$ is the *z*-directional component of the $\underline{q}^{\mathrm{b}}$, which is the position vector of the *j*th element of the spar with respect to the spar frame. The added moment M_A^{b} is valid only when the *j*th element of the spar is submerged in fluid.

2.2 Cable modeling

Based on the research by ZHU, et al[13–14], the cable is simplified using the lumped-mass-and-spring modeling scheme, wherein the cable is divided into N elements ordered from the top to the bottom, as shown in Fig. (1). The previous paper developed a new element-fixed frame by which the formulations of both the rotational transformation matrix and the external forces are effectively expressed. Element position vector $\underline{E}_g^i$ is expressed by the positions of the terminal nodes, as given by Eq. (7). Relative velocity $\underline{V}_g^R$ is the mean value of the relative velocities acting on the terminal nodes, as given by Eq. (8). $\underline{\dot{N}}_g^i$ is the velocity of the *i*th node:

$$\underline{E}_g^i = \underline{N}_g^{i+1} - \underline{N}_g^i, \tag{7}$$

$$\begin{aligned} \underline{V}_g^R &= \frac{\underline{V}_g^{i+1} + \underline{V}_g^i}{2}, \\ \underline{V}_g^i &= \underline{V}_g^f - \underline{\dot{N}}_g^i, \end{aligned} \tag{8}$$

$$\begin{aligned} \overline{z}^i &= \frac{\underline{E}_g^i}{\left\| \underline{E}_g^i \right\|}, \\ \overline{x}^i &= \frac{\tilde{z}^i \underline{V}_g^R}{\left\| \tilde{z}^i \underline{V}_g^R \right\|}, \\ \overline{y}^i &= \tilde{z}^i \overline{x}^i. \end{aligned} \tag{9}$$

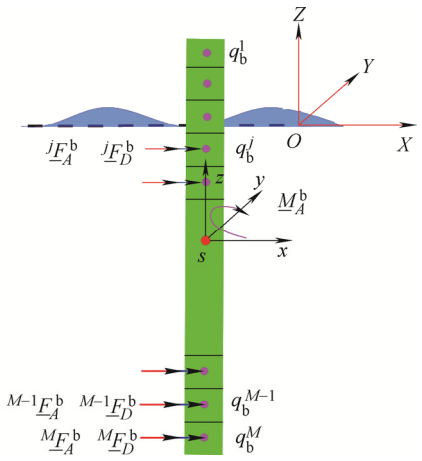

Fig. 3. Element modeling of spar

Unit axis $\overline{z}^i$ directs the orientation of the *i*th element and is obtained by unitizing the element position vector $\underline{E}_g^i$, as illustrated in Fig. 4. Unit axis $\overline{x}^i$ is perpendicular to plane P_1, which is composed of unit axis $\overline{z}^i$ and relative velocity $\underline{V}_g^R$. According to the right-hand principle, unit axis $\overline{y}^i$ is perpendicular to plane P_2, which is composed of unit axes $\overline{z}^i$ and $\overline{x}^i$. The unit axes of the *i*th element are given specifically by Eq. (9).

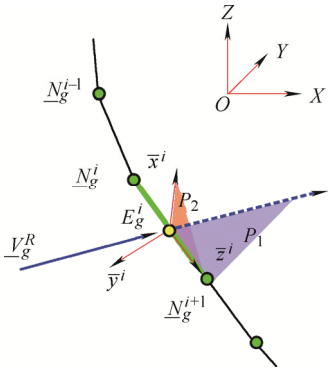

Fig. 4.　Element-fixed reference frame

The forces acting on the cable include the stiffness of the cable $\underline{T}_b^i$, damping of the cable $\underline{D}_b^i$, hydrodynamic drag forces F_z^i and F_y^i, and apparent weight $\underline{F}_W^i$. These forces are expressed in detail in references[13–14] and are briefly listed in Eq. (10):

$$\begin{aligned}
\underline{T}_b^i &= \frac{\pi d_c^2}{4} E \varepsilon_b^i \bar{z}, \\
\underline{D}_b^i &= C_d \underline{\underline{A}}^{iT} \left(\dot{N}_g^{i+1} - \dot{N}_g^i \right) \bar{z}, \\
F_z^i &= \frac{\pi}{2} C_{\mathrm{f}} \rho_{\mathrm{f}} d^i l^i \left\| \underline{V}_g^R \right\| \bar{z}^T \underline{V}_g^R, \\
F_y^i &= -\frac{1}{2} C_n \rho_{\mathrm{f}} d^i l^i \left\| \underline{V}_g^R \right\| \bar{x}^{\mathrm{T}} \left(\bar{z} \underline{V}_g^R \right), \\
\underline{F}_{\mathrm{W}}^i &= \left(m_{\mathrm{c}}^i - m_{\mathrm{f}}^i \right) \underline{g},
\end{aligned} \tag{10}$$

where ε_b^i is the axial strain, l^i represents the length of the ith cable element, and the masses of the cable and the displaced fluid for the ith element m_{c}^i and m_{f}^i are given by

$$\begin{aligned}
\varepsilon_b^i &= \frac{l^i - l_0^i}{l_0^i} \\
l^i &= \sqrt{\underline{E}_g^{iT} \underline{E}_g^i} \\
m_{\mathrm{c}}^i &= \frac{\pi d_c^2}{4} l_0^i \rho_{\mathrm{c}} \\
m_{\mathrm{f}}^i &= \frac{\pi d_c^2}{4} l_0^i \rho_{\mathrm{f}}
\end{aligned} \tag{11}$$

The mass matrix of the ith element with respect to the element-fixed frame is given by Eq. (12). The added mass effect along the cable axial is ignored.

$$M_b^i = \begin{pmatrix} m_{\mathrm{c}}^i + C_A m_{\mathrm{f}}^i & 0 & 0 \\ 0 & m_{\mathrm{c}}^i + C_A m_{\mathrm{f}}^i & 0 \\ 0 & 0 & m_{\mathrm{c}}^i \end{pmatrix}. \tag{12}$$

Mass matrixes of the nodes with respect to the global reference frame are expressed by mass matrixes of the elements with respect to the local reference frame. Here, the mass matrix of the ith node M_I^i is composed of the element-mass matrixes M_b^{i-1} and M_b^i, and is given by

$$M_I^i = \frac{1}{2} \underline{\underline{A}}^{i-1} M_b^{i-1} \underline{\underline{A}}^{i-1\ \mathrm{T}} + \frac{1}{2} \underline{\underline{A}}^i M_b^i \underline{\underline{A}}^{i\ \mathrm{T}}. \tag{13}$$

Finally, the forces acting on each cable element are shared equally by the element-terminal nodes. The governing equation for the ith node is defined by the forces acting on the $(i-1)$th and ith element, as given by Eq. (14). The bottom of the cable is fixed to the seabed with spring forces T^{spr} and the first node of the cable is connected to the bottom of the floating platform with a spherical joint. The properties of the cable in this modeling are shown in Table 2.

$$\begin{aligned}
M_I^i \ddot{N}_g^i = \underline{\underline{A}}^i \left(T_b^i + D_b^i + \frac{1}{2} F_D^i \right) - \underline{\underline{A}}^{i-1} \left(T_b^{i-1} + D_b^{i-1} - \frac{1}{2} F_D^{i-1} \right) + \\
\frac{1}{2} \left(F_W^i + F_W^{i-1} \right)
\end{aligned} \tag{14}$$

Table 2.　Properties of cable

Parameter	Value
Diameter d_c /m	0.03
Density ρ_c /(kg • m^{-3})	1570
Elastic modulus E/GPa	2.38
Damping C_d /(N • s • m^{-1})	1800
Drag coef. in transversal direction C_n	1
Drag coef. in longitudinal direction C_{f}	0.5
Added-mass coefficient C_A	1
Position of top node $\underline{N}_g^1$ /m	(0, 0, –4.5)
Position of bottom node $\underline{N}_g^N$ /m	(0, 0, –30)

2.3　Constraint Modeling

The constraint modeling defined here is used for connecting two independent bodies.

2.3.1　Spherical joint

A rigid body has DOFs(six degree of freedoms) in three dimensions, while a mass point only has three translational DOFs. Three-dimensional spherical joint modeling was well developed in references[23–24], but an applicable modification is needed for connecting the spar and cable, because the cable is composed of nodes that only have three translational DOFs. The constraint equation $\underline{\Phi}^{\mathrm{sph}}$ is expressed by

$$\underline{\Phi}^{\mathrm{sph}} = \underline{q}^{\mathrm{b}} + \underline{\underline{A}}^{\mathrm{b}} \underline{s}_k'^{\mathrm{b}} - \underline{q}^1, \tag{15}$$

where $\underline{q}^{\mathrm{b}}$ denotes the origin of the local frame of the spar with respect to the global frame, and $\underline{\underline{A}}^{\mathrm{b}}$ denotes the rotational transformation matrix of the spar. The vector $\underline{s}_k'^{\mathrm{b}}$ denotes the position of a joint point with respect to the local frame of the spar platform. Because it is the *1*st node of the cable that connects to the spar platform, $\underline{q}^1$ denotes

the position of the *1*st node of the cable with respect to the global reference frame.

$\underline{\underline{\boldsymbol{\Phi}}}_q^{\text{sph}}$ denotes the Jacobian matrix of the constraint equation and is shown by

$$\underline{\underline{\boldsymbol{\Phi}}}_q^{\text{sph}} = \begin{pmatrix} \underline{\underline{I}} & -\underline{\underline{A}}^{\text{b}} \underline{\underline{\tilde{s}}}_k'^{\text{b}} \underline{\underline{G}}'^{\text{b}} & -\underline{\underline{I}} \end{pmatrix}, \tag{16}$$

where $\underline{\underline{G}}'^{\text{b}}$ is used to express the relation between the angular velocities and Euler angles, as instructed by SHABANA[24]. The *Z-Y-X* Euler angle set is adopted in this paper, where $\underline{\underline{G}}'^{\text{b}}$ can be carried out according to the research by GREENWOOD[25]; and $\underline{\underline{\tilde{s}}}_k'^{\text{b}}$ represents the skew symmetric of the body vector $\underline{\underline{\tilde{s}}}_k'^{\text{b}}$.

γ is used to satisfy the derivation of the constraint equations according to NIKRAVESH[23]. It is composed of the displacements and first derivation of the displacements with respect to time, and is given by

$$\gamma = \left(\underline{\underline{A}}^{\text{b}} \underline{\underline{\tilde{\omega}}}'^{\text{b}} \underline{\underline{\tilde{s}}}_k'^{\text{b}} \underline{\underline{G}}'^{\text{b}} + \underline{\underline{A}}^{\text{b}} \underline{\underline{\tilde{s}}}_k'^{\text{b}} \dot{\underline{\underline{G}}}'^{\text{b}} \right) \dot{\underline{\theta}}^{\text{b}}. \tag{17}$$

2.3.2 Spring forces

The spring forces are linear function of the relative positions and velocities between the bottom node of the cable q^{N+1} and the anchor point P^{anchor} on the seabed. They are used to fix the cable on the seabed. The spring forces are carried out using three-by-three coefficient matrixes $\boldsymbol{K}$ and $\boldsymbol{C}$, as shown by

$$T^{\text{spr}} = \boldsymbol{K}\left(q^{N+1} - P^{\text{anchor}}\right) + \boldsymbol{C}\left(\dot{q}^{N+1} - \dot{P}^{\text{anchor}}\right) \tag{18}$$

where $\boldsymbol{K}$ and $\boldsymbol{C}$ are three-by-three coefficient matrixes of the stiffness and damping, respectively. Both of them are diagonal matrixes and are composed of coefficients k_{s} and c_{s}, respectively. The values are listed in Table 3.

Finally, the equation of motion of the constrained system can be expressed by

$$\begin{pmatrix} M & \left(\boldsymbol{\Phi}_q^{\text{sph}}\right)^{\text{T}} \\ \boldsymbol{\Phi}_q^{\text{sph}} & 0 \end{pmatrix} \begin{pmatrix} \ddot{q} \\ \lambda \end{pmatrix} = \begin{pmatrix} Q \\ \gamma \end{pmatrix}, \tag{19}$$

where $\boldsymbol{M}$ is the mass matrix of the system, and Q is the external forces of the system. The matrix $\left(\boldsymbol{\Phi}_q^{\text{sph}}\right)^{\text{T}}$ denotes the transposed Jacobian matrix.

Table 3. Parameters of spring forces

Parameter	Value
Stiffness k_{s} /(MN • m^{-1})	87.0
Damping c_{s} /(MN • s • m^{-1})	33.0

2.4 Ocean Modeling

The linear wave theory by JOURNEE[15] is used to express surface waves in this paper. The amplitude of the surface waves is a function of the time and positions as shown in

$$\zeta = \zeta_a \cos\left(kX_g - \omega t\right). \tag{20}$$

With the assumption of an infinite water depth, the velocities and accelerations of the water particles can be found according to Eqs. (21), (22), respectively. Therefore, the velocities and accelerations of water particles matching positions of both the cable and spar elements can be found for the calculation of the hydrodynamic loads.

$$\begin{aligned} u_g &= \zeta_a \bullet \omega \bullet \mathrm{e}^{kZ_g} \cos\left(kX_g - \omega t\right), \\ w_g &= \zeta_a \bullet \omega \bullet \mathrm{e}^{kZ_g} \sin\left(kX_g - \omega t\right), \end{aligned} \tag{21}$$

$$\begin{aligned} \dot{u}_g &= \zeta_a \bullet \omega^2 \bullet \mathrm{e}^{kZ_g} \sin\left(kX_g - \omega t\right), \\ \dot{w}_g &= -\zeta_a \bullet \omega^2 \bullet \mathrm{e}^{kZ_g} \cos\left(kX_g - \omega t\right). \end{aligned} \tag{22}$$

In addition, the wave length λ, wave numbers k, and circular wave frequency ω can be found according to

$$\lambda = \frac{\|g\| T^2}{2\pi}; k = \frac{2\pi}{\lambda}; \omega^2 = k\|g\|, \tag{23}$$

where T is the wave period, and ζ_a denote wave amplitude. All the parameters for the sea state are listed in Table 4.

Table 4. Sea state parameters

Parameter	Value
Wave amplitude ζ_a /m	0.7
Wave period T /s	6.4
Current $\underline{V}_g^c$ /(m • s^{-1})	(0.5, 0, 0)
Water density ρ_{f} /(kg • m^{-3})	1025

In this paper, the current is set as a constant velocity. Finally, the velocity of the fluid $\underline{V}_g^{\text{f}}$, is composed of the wave velocity $\underline{V}_g^{\text{w}}$ and current velocity $\underline{V}_g^{\text{c}}$ as given by

$$\underline{V}_g^{\text{f}} = \underline{V}_g^{\text{w}} + \underline{V}_g^{\text{c}} \tag{24}$$

where $\underline{V}_g^{\text{w}} = \begin{pmatrix} u_g & 0 & w_g \end{pmatrix}^{\text{T}}$

3 Simulation Results

This numerical modeling scheme was coded using MATLAB 2012 and verified in comparison with the commercial simulation code ProteusDS. The Runge-Kutta algorithm was chosen as the integrator, and the total simulation time was set as 200 s in here. All the simulation

conditions were consistent with those in ProteusDS. The simulation results from the numerical modeling are compared with those from ProteusDS. In view of the limitation that all the external loads were applied in *X*-direction, the surge, heave and pitch motions are important parameters in analyzing the motions of the floating spar. This paper also analyzes the forces acting on the spar and the tensions within the cable. Finally, the frequency of the tension within the cable and frequency of the spar motions are illustrated. Measure point is the origin of the local reference frame of the spar.

The comparisons of the surge and heave motions are shown in Figs. 5, 6, respectively. Even though the results are consistent at the end of the simulation, the reaction of the numerical modeling is quicker than that by ProteusDS. In addition to the forces listed in the front part of this paper, it is predicted an additional damping is applied to counter the motion of the spar platform in ProteusDS. The load-displacement relationships are also analyzed by this paper according to the results of the numerical modeling. The restoring moment is directly related to the rotational motions of the spar such as the pitch motion, as illustrated in Figs. 7, 8. The entire external loads are calculated by adding up loads acting on the cylinder elements in numerical modeling, while the small tetrahedron elements are used in ProteusDS. The numerical modeling is more efficient than the ProteusDS. The efficiency comes from the assumption that the wetted cross curve is a plane, and this assumption is available with small pitch angles, as shown in Fig. 7. This simplification will be verified further with a real experiment.

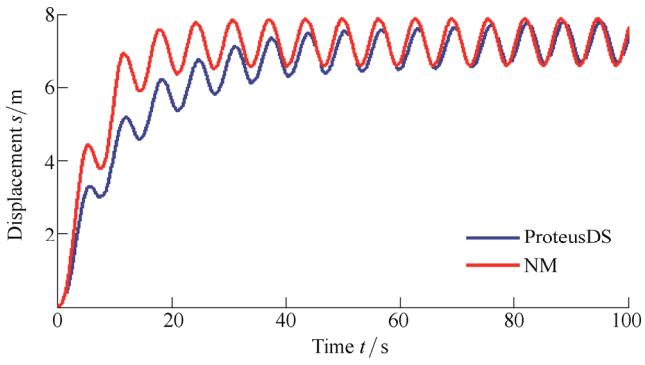

Fig. 5.　Surge motion of the spar

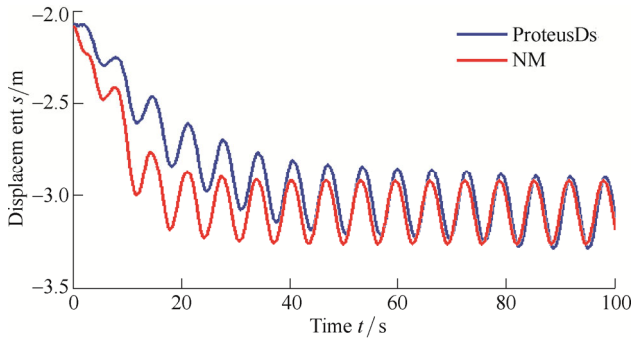

Fig. 6.　Heave motion of the spar

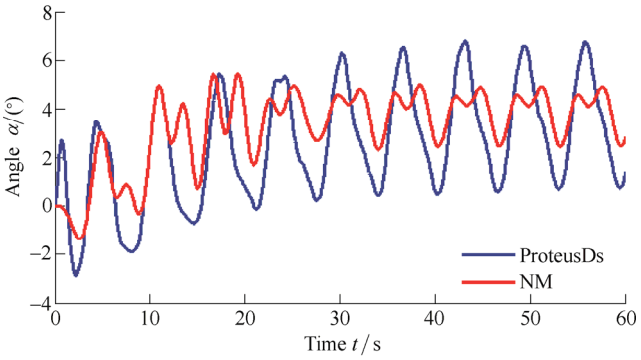

Fig. 7.　Pitch motion of the spar

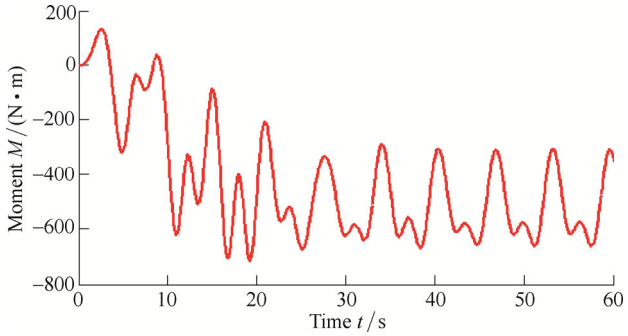

Fig. 8.　Restoring moment of the spar about Y-axis

The restoring moments are sensitive to the geometry of the spar platform, especially, the position of the center of mass. The propagating wave forces the hydrodynamic drag forces oscillating with an amplitude of 200 N, while the current has a constant effect and enables the mean value of the hydrodynamic drag forces being about 300 N, as shown in Fig. 9. Hydrodynamic drag forces have dominant effect on the surge and heave motions of the spar. The crest of the buoyancy is limited to a value of 6318N, as shown in Fig. 10. This phenomenon indicates that the spar is fully submerged at that time. This unsmooth change causes oscillations at the crest of the tensions as shown in Fig. 11. Because the cable is fixed on the bottom of the spar, the cable tension is directly affected by the pitch motion of the spar. This effect is reflected in the numerical modeling rather than in ProteusDS. The prediction of additional damping in ProteusDS also hold true in here. The pitch motion and restoring moment oscillate heavily when the simulation time ranges from the 10th second to the 20th second. This phenomenon indicates that the system is reaching equilibrium under the constraint of cable and effects of wave and current. The effects of wave and current is much larger than the constraint of cable at the beginning, and the spar is accelerated in the *X*-direction. With the *X*-directional moving of the spar, the tension within the cable increases and tends to balance the effects of wave and current. This phenomenon is also obviously reflected in the surge and heave motions and tensions within the cable. The surge and heave motions decelerates as shown in Figs. 5, 6, respectively, and the tension rapidly increased, as shown in Fig. 11.

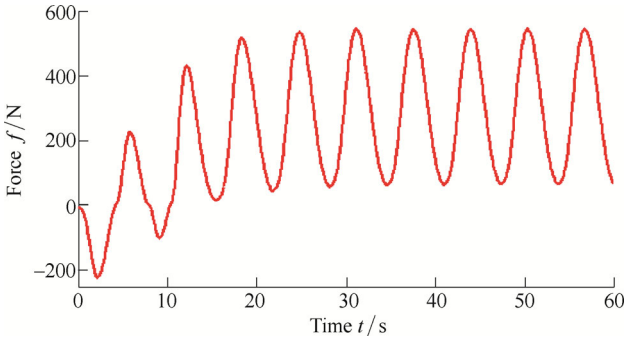

Fig. 9. Hydrodynamic drag force of the spar along X-axis

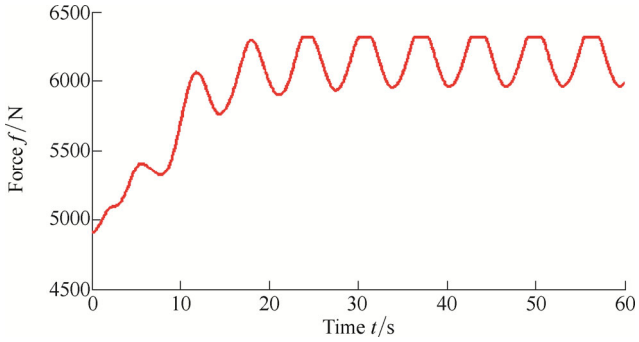

Fig. 10. Buoyancy of the spar

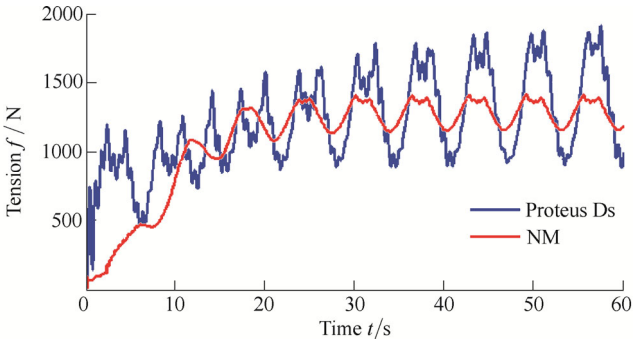

Fig. 11. Tension within cable

Because the period of the X-directional wave is 6.4 s, the frequency of the wave is 0.156 HZ. The frequencies of the surge motions are similar with those of the heave motions, only the frequency of the surge motions are shown in Fig. 12 which is greatly influenced by the frequency of the propagating wave. The frequency of the pitch motion is also affected by the frequency of the wave and tension forces, as shown in Figs. 13, 14, respectively.

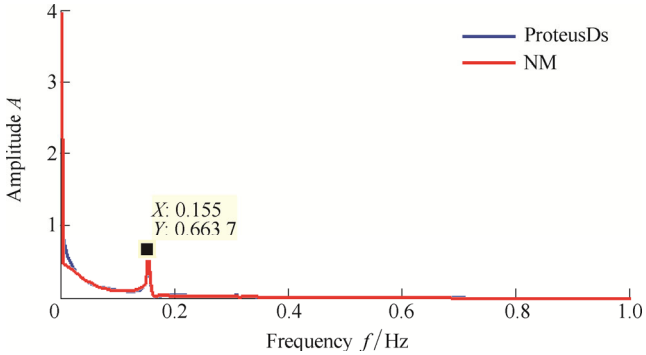

Fig. 12. Frequency of surge motion of the spar

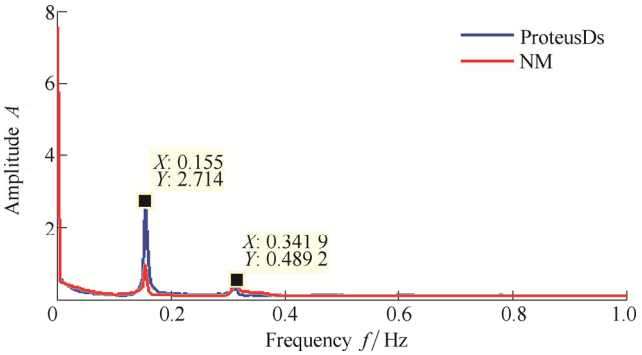

Fig. 13. Frequency of pitch motion of the spar

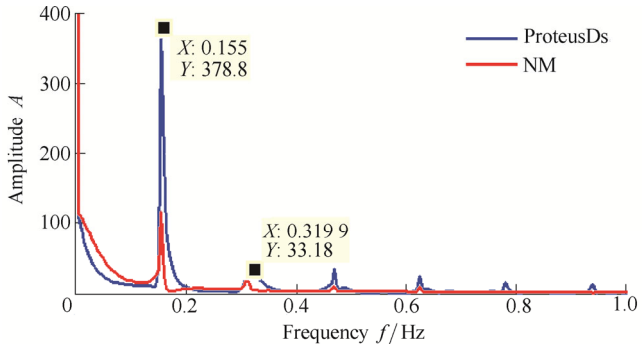

Fig. 14. Frequency of tension within cable

4 Conclusions

(1) The numerical modeling of a platform tethered by a mooring cable through a spherical joint is well developed and verified with ProteusDS. This numerical modeling contributes to the development of virtual simulation software in mechanical engineering.

(2) The dynamic responses of the spar with the wave and current are analyzed, and these responses are significate for the optimization design of the floating structure.

(3) The wave load has the dominant influence on the surge and heave motions of the spar, and the pitch motion has an obvious effect on the tension within the cable.

(4) The phenomenon of achieving dynamic equilibrium has an obvious effect on the pitch motion, while it has less effect on the heave and surge motions.

(5) The phenomenon of being fully submerged has an obvious effect on the pitch motion and tension within the cable.

References

[1] JOHNSON K R, KERR S, SIDE J C. Marine renewable and coastal communities-experiences from the offshore oil industry in the 1970s and their relevance to marine renewables in the 2010s[J]. *Marine Policy*, 2013, 38: 491–499.

[2] DRISCOLL F R, LUECK R G, NAHON M. Development and validation of a lumped-mass dynamics model of a deep-sea ROV system[J]. *Applied Ocean Research,* 2000, 22: 169–182.

[3] MERCHANT H C, KELF M A. Non-linear analysis of submerged ocean buoy systems[C]//*Proceedings of MTS/IEEE Oceans 73,* 1973, 1: 390–395.

[4] OGIHARA K. Theoretical analysis on the transverse motion of a buoy by surface wave[J]. *Applied Ocean Research,* 1980, 2(2): 51–56.

[5] DRISCOLL R, NAHON M. Mathematical modeling and simulation of a moored buoy system[J]. *IEEE,* 1996: 517–523.
[6] AGARWAL A K, JAIN A K. Dynamic behavior of offshore spar platforms under regular sea waves[J]. *Ocean Engineering*, 2003, 30: 487–516.
[7] IDRIS K, LEONARD J W, YIM S C S. Coupled dynamics of tethered buoy system[J]. *Ocean Engineering*, 1997, 24(5): 445–464.
[8] RADHAKRISHNAN S, DATLA R, HIRES R I. Theoretical and experimental analysis of tethered buoy instability in gravity waves[J]. *Ocean Engineering*, 2007, 34: 261–274.
[9] VERITAS D N. Numerical models for SPAR platform dynamics[C]// *Proceeding of the thirteenth(2003) international offshore and polar engineering conference*, Honolulu, Hawaii, USA, May 25–30, 2003.
[10] KOO B J, KIM M H, RANDALL R E. Mathieu instability of spar platform with mooring and risers[J]. *Ocean Engineering*, 2004, 31: 2175–2208.
[11] ZHU X Q, KIM H W, YOO W S. Dynamic analysis of an offshore wind turbine with a spar-type platform[C]//*Proceedings of 6th Asian Conference on Multibody Dynamic*, Shanghai, China, Aug. 26–30, 2012.
[12] JONKMAN J. Definition of the floating system for phase IV of OC3[R]. *Technical Report NREL/TP–500–47535*, 2010.
[13] ZHU X Q, BAUCHAU O A, YOO W S. Dynamic analysis of mooring cable fastening a floating sphere on the ocean[C]// *Proceedings of ASME 2013 International Design Engineering Technical Conferences & Computers and Information in Engineering Conference*, Portland, Oregon, USA, August 4–7, 2013, DETC2013/12693.
[14] ZHU X Q, YOO W S. New construction of reference frame for underwater cable[C]//*Proceeding of the ASME 2014 33rd international conference on Ocean, offshore and Arctic Engineering OMAE2014,* San Francisco, California, USA, June 8–13, 2014, OMAE2014/24297.
[15] JOURNEE J M J, MASSIE W W. *Offshore hydromechanics*[M]. 1st ed. Delft: Delft University of Technology, 2001.
[16] DSA PACIFIC, *ProteusDS 2013 manual*[R]. Dynamic System Analysis Ltd, 2013.
[17] DSA PACIFIC, *ProteusDS theory and validation*[R]. Dynamic System Analysis Ltd, 2014.
[18] BAUCHAU O A. *Flexible multibody dynamics*[M]. Netherlands: Springer Science + Business Media B.V., 2011.
[19] WALTON T S, POLACHEK H. Calculation of transient motion of submerged cables[J]. *Mathematics of Computation*, 1960, 14(69): 27–46.
[20] BUCKHAM B J. *Dynamics modeling of low-tension tethers for submerged remotely operated vehicles*[D]. A thesis submitted in partial fulfillment of the requirements for the degree of Doctor of Philosophy in Department of Mechanical Engineering, University of Victoria, 2003.
[21] PARK H H. A tension measurement method of a towing cable or a buoy cable[J]. *Ocean Engineering*, 1993, 20 (2): 163–170.
[22] HUANG S. Dynamic analysis of three-dimensional marine cable[J]. *Ocean Engineering*, 1994, 21(6): 587–605.
[23] NIKAVESH P E. *Computer-aided analysis of mechanical systems*[M]. Upper Saddle River: Prentice-Hall, Inc., 1988.
[24] SHABANA A A. *Computational dynamics*[M]. 3rd ed. Hoboken: John Wiley & Sons, Inc., 2010.
[25] GREENWOOD D T. *Principles of dynamics*[M]. 2nd ed. Upper Saddle River: Prentice-Hall, Inc., 1988.

Biographical notes

ZHU Xiangqian, born in 1987, is currently a PhD candidate at *Computer Aided Engineering Laboratory, Pusan National University, Korea.* He received his master degree from *Pusan National University, South Korea*, in 2010. His research interests include dynamics of flexible multibody system, ocean engineering, and numerical modeling of floating platform.
E-mail: zhuxiangqian@pusan.ac.kr

YOO Wan-Suk, born in 1954, is currently a professor and the director at *NRL (National Research Laboratory) of Computer Aided Engineering, Pusan National University, Korea.* His main research interests include dynamics of flexible multibody system, vehicle dynamics, dynamics simulation and application.
E-mail: wsyoo@pusan.ac.kr